

Extension of the energy range of the experimental activation cross-sections data of longer-lived products of proton induced nuclear reactions on dysprosium up to 65 MeV

F. Tárkányi^a, F. Ditrói^{a,*}, S. Takács^a, A. Hermanne^b, A.V. Ignatyuk^c

^a*Institute for Nuclear Research, Hungarian Academy of Sciences (ATOMKI), Debrecen, Hungary*

^b*Cyclotron Laboratory, Vrije Universiteit Brussel (VUB), Brussels, Belgium*

^c*Institute of Physics and Power Engineering (IPPE), Obninsk, Russia*

Abstract

Activation cross-sections data of longer-lived products of proton induced nuclear reactions on dysprosium were extended up to 65 MeV by using stacked foil irradiation and gamma spectrometry experimental methods. Experimental cross-sections data for the formation of the radionuclides ^{159}Dy , ^{157}Dy , ^{155}Dy , ^{161}Tb , ^{160}Tb , ^{156}Tb , ^{155}Tb , $^{154m2}\text{Tb}$, $^{154m1}\text{Tb}$, ^{154g}Tb , ^{153}Tb , ^{152}Tb and ^{151}Tb are reported in the 36-65 MeV energy range, and compared with an old dataset from 1964. The experimental data were also compared with the results of cross section calculations of the ALICE and EMPIRE nuclear model codes and of the TALYS nuclear reaction model code as listed in the latest on-line libraries TENDL 2013.

Keywords: dysprosium target, stacked-foil technique, proton activation, excitation function, integral yield

1. Introduction

In the frame of this systematic study we have investigated the activation cross sections induced by protons and deuterons on natural dysprosium targets. The part of the study specifically devoted to production of ^{161}Ho , a candidate therapeutic radioisotope, was published separately (Tárkányi et al., 2013a). Activation cross-sections of long-lived products of deuteron induced nuclear reactions on dysprosium up to 50 MeV was published in (Tárkányi et al., 2014a) and of proton induced nuclear reactions on dysprosium up to 36 MeV in (Tárkányi et al., 2013b). Recently we had the possibility to perform the same measurements at higher energies. Here we report on the activation cross section data induced by proton irradiation of dysprosium in the 36-65 MeV energy range. Only one set of earlier experimental data were found in the literature (May and Yaffe, 1964).

2. Experiment and data evaluation

For the cross section determination an activation method based on stacked foil irradiation technique fol-

lowed by γ -ray spectroscopy were used. The general characteristics and procedures for irradiation, activity assessment and data evaluation (including estimation of uncertainties) were similar as in many of our earlier works (Tárkányi et al., 2013a,b, 2014a). The stack consisted of a sequence of Al, Dy, Al, Hf, Al, Ti, Be, Ti foils repeated 25 times and bombarded for 3600 s with a 65 MeV proton beam of 25 nA at Louvain la Neuve in one single irradiation. From this irradiation the activation cross sections for production of ^7Be by proton up to 65 MeV were already published, where additional details can be found on experiment on beam parameters and on the data evaluation (Hermanne et al., 2014). The main experimental parameters and the methods of data evaluation for the present study are summarized in Table 1. The used decay data are collected in Table 2.

For beam current and beam energy monitoring, for energy degradation and recoil catcher Al and Ti foils were incorporated downstream of each dysprosium foils in the stack. All monitor foil data were considered simultaneously in order to obtain the beam current and beam energy in each target foil by comparison with the IAEA recommended monitor data (Tárkányi et al., 2001). The measured cross sections of the monitor reaction $^{27}\text{Al}(p,x)^{22,24}\text{Na}$ and the recommended data are

*Corresponding author: ditroi@atomki.hu

Table 1: Main parameters of the experiment and the methods of data evaluations

Experiment		Data evaluation	
Incident particle	Proton	Gamma spectra evaluation	Genie 2000, (Canberra, 2000), Forgamma (Székely, 1985)
Method	Stacked foil	Determination of beam intensity	Faraday cup (preliminary) Fitted monitor reaction (final) (Tárkányi et al., 1991)
Target stack and thicknesses	Al(49.6 μm), Dy(22.1 μm), Al(98 μm), Hf(107 μm), Al(49.6 μm), Ti(10.9 μm), Be(285 μm), Ti(10.9 ν) block Repeated 25 times	Decay data	NUDAT 2.6 (Kinsey et al., 1997)
Number of target foils	25x8	Reaction Q-values	Q-value calculator (Pritychenko and Sonzogni, 2003)
Accelerator	Cyclone 90 cyclotron of the Université Catholique in Louvain la Neuve (LLN) Belgium	Determination of beam energy	Andersen (Andersen and Ziegler, 1977) (preliminary) Fitted monitor reaction (final) (Tárkányi et al., 2001)
Primary energy	65 MeV	Uncertainty of energy	Cumulative effects of possible uncertainties (International-Bureau-of-Weights-and-Measures, 2000)
Irradiation time	60 min	Cross sections	Elemental cross section
Beam current	25 nA	Uncertainty of cross sections	Sum in quadrature of all individual contribution
Monitor reaction, [recommended values]	$^{nat}\text{Ti}(p,x)^{48}\text{V}$ $^{27}\text{Al}(p,x)^{22,24}\text{Na}$ reactions	Yield	Physical yield (Bonardi, 1987)
Monitor target and thickness	^{nat}Ti , 10.9 μm ^{27}Al 98 μm	Theory	ALICE-IPPE (Dityuk et al., 1998) ,EMPIRE (Herman et al., 2007); (Koning and Rochman, 2012) ,TALYS (Koning et al., 2012)
detector	HPGe		
γ -spectra measurements	4 series		
Cooling times (h)	22.0-31.6 71.6-96.2 140.6-333.8 2638-3213		

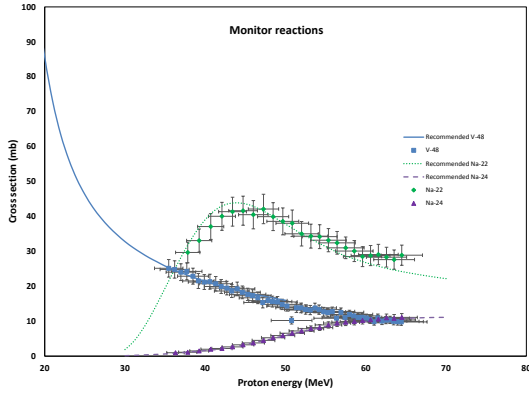


Figure 1: The simultaneously measured monitor reactions for determination of proton beam energy and intensity

shown in Fig. 1.

3. Results and discussion

3.1. Cross sections

The measured cross sections for the production of ^{159}Dy , ^{157}Dy , ^{155}Dy , ^{161}Tb , ^{160}Tb , ^{156}Tb , ^{155}Tb , $^{154m2}\text{Tb}$, $^{154m1}\text{Tb}$, ^{154g}Tb , ^{153}Rb , ^{152}Tb and ^{151}Tb are shown in Table 3-4 and Figures 2-14. The figures also show the theoretical results calculated with the ALICE-IPPE and the EMPIRE codes and the values available in the TALYS based TENDL-2013 library in comparison with experimental results of this work. In this case we also

used the opportunity to compare the results of the older EMPIRE-IPPE version with the newest EMPIRE 3.2 (Malta) (Herman et al., 2014) calculations. Due to the experimental circumstances (stacked foil technique, large dose at EOB, limited detector capacity) no cross section data were obtained for short-lived Ho activation products. Naturally occurring dysprosium is composed of 7 stable isotopes (^{156}Dy -0.06 %, ^{158}Dy -0.10 %, ^{160}Dy -2.34 %, ^{161}Dy -18.9 %, ^{162}Dy -25.5 %, ^{163}Dy -24.9 % and ^{164}Dy -28.2 %). The relevant contributing reactions are collected in Table. 2.

Radioisotopes of dysprosium

The investigated radioisotopes of dysprosium are produced directly via (p,pxn) reactions and from the decay of the simultaneously produced holmium parent isotopes.

3.1.1. The $^{nat}\text{Dy}(p,x)^{159}\text{Dy}$ reaction

The cumulative cross sections of the ^{159}Dy ($T_{1/2} = 144.4$ d) contain, apart from the direct production, the contribution from the decay of ^{159}Ho ($T_{1/2} = 33.05$ min) as they were measured after nearly complete decay of the parent isotope. A very old dataset of (May and Yaffe, 1964) show acceptable agreement with our new data up to 60 MeV. The agreement with the results of the 3 codes is also acceptable (Fig. 2), the best approximation is given by the TENDL up to 40 MeV. According to the theory the direct production is negligible, especially below 30 MeV.

3.1.2. The $^{nat}\text{Dy}(p,x)^{157}\text{Dy}$ reaction

The cumulative cross sections for production of ^{157}Dy ($T_{1/2} = 8.14$ h) was measured after nearly com-

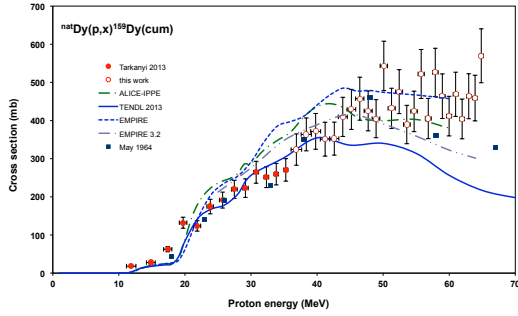


Figure 2: Experimental and theoretical cross sections for the formation of ^{159}Dy by the proton bombardment of dysprosium

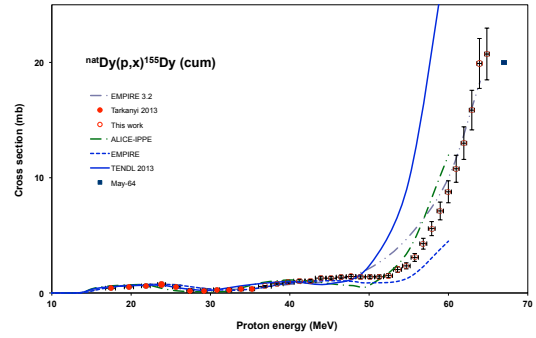


Figure 4: Experimental and theoretical cross sections for the formation of ^{155}Dy by the proton bombardment of dysprosium

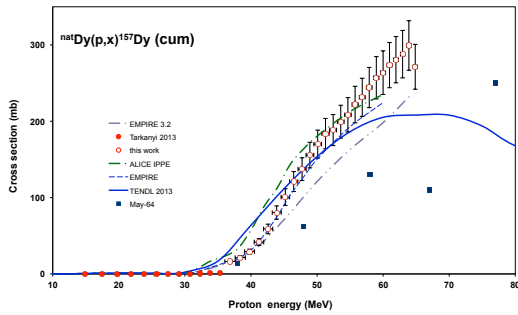


Figure 3: Experimental and theoretical cross sections for the formation of ^{157}Dy by the proton bombardment of dysprosium

plete decay of the parent ^{157}Ho ($T_{1/2} = 12.6$ min) (Fig. 3.) The data of May from 1964 are much lower than ours above 40 MeV. The best theoretical approximation is given by the EMPIRE in the whole energy range, ALICE-IPPE also gives good results above 50 MeV, while surprisingly the EMPIRE 3.2 underestimates above 45 MeV. The direct production is negligible.

3.1.3. The $^{nat}\text{Dy}(p,x)^{155}\text{Dy}$ reaction

The measured ^{155}Dy ($T_{1/2} = 9.9$ h) was produced directly and through the decay of the ^{155}Ho , ($T_{1/2} = 48$ min) parent radioisotope. From the former dataset of May only one point overlaps with our measurements showing an acceptable agreement. The comparison with the theoretical calculations shows disagreement above

50 MeV (Fig. 4), especially TENDL shows a strong overestimation, but the new EMPIRE 3.2 version shows acceptable agreement.

Radioisotopes of terbium

The terbium radioisotopes are produced through directly $(p,2pxn)$ reactions (including complex particle emissions) and decay of simultaneously produced dysprosium radio-products.

3.1.4. The $^{nat}\text{Dy}(p,x)^{161}\text{Tb}$ reaction

The measured direct cross sections for production of ^{161}Tb ($T_{1/2} = 6.89$ d) are shown in Fig. 5 in comparison with the theoretical predictions. As can be seen in Table 2, reactions on stable Dy target isotopes with nearly the same abundance can contribute to the production of ^{161}Tb . From systematics it is known that the $(p,2p)$ reaction has mostly lower cross sections than the $(p,2pn)$ channel. The sharp low energy peak due to $^{162}\text{Dy}(p,2p)$ that can be seen in the TENDL theoretical data is hence questionable and is reproduced neither by the experimental values, nor by the EMPIRE and ALICE results. In the high-energy range there are large disagreements between the theoretical results. The trend of the experimental data in this energy range support the TENDL calculations, but the new EMPIRE 3.2 gives better approach below 50 MeV. Unfortunately our previous and present data connect at the point, where the cross section begins to increase starkly, as well as because of the low statistic the last points of the present stack are not so reliable, which facts result in a disagreement in the connection range.

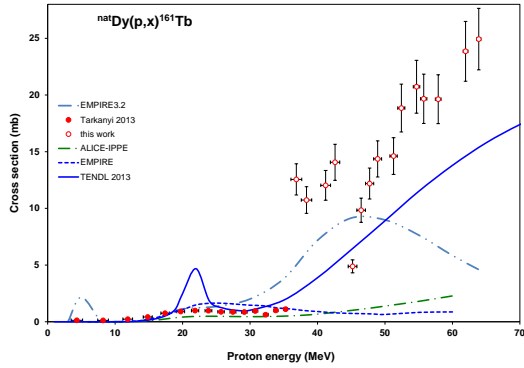


Figure 5: Experimental and theoretical cross sections for the formation of ^{161}Tb by the proton bombardment of dysprosium

3.1.5. The $^{nat}\text{Dy}(p,xn)^{160}\text{Tb}$ reaction

The new experimental data of the ^{160}Tb ($T_{1/2} = 72.3$ d) are in good agreement with the low energy data in the overlapping energy range. The theoretical descriptions seem to be not very successful (Fig. 6). The sharp peak predicted by the TENDL is not present in the excitation function. The shape of the excitation function is more or less described only by ALICE-IPPE, but the magnitudes are significantly differ from the experimental data in the whole energy range.

3.1.6. The $^{nat}\text{Dy}(p,xn)^{156}\text{Tb}$ reaction

The cross sections of ^{156g}Tb ($T_{1/2} = 5.35$ d) were obtained from spectra measured after the complete decay of the two short-lived isomeric states ($T_{1/2} = 5.3$ h, IT: 100 % and $T_{1/2} = 24.4$ h, IT: 100 %). In the investigated energy range the ALICE-IPPE represents very closely the experimental data (Fig. 7), the TENDL results underestimate, while both EMPIRE versions overestimate the experimental cross sections by at least a factor of 3.

3.1.7. The $^{nat}\text{Dy}(p,xn)^{155}\text{Tb}$ reaction

The measured cumulative cross sections of ^{155}Tb ($T_{1/2} = 5.32$ d) contains the complete contribution from the decay of ^{155}Dy ($T_{1/2} = 9.9$ h). The agreement of by the theories predicted cross sections with the experimental data is shown in Fig. 8. Only the ALICE-IPPE and TENDL codes give acceptable approximation above 55 MeV.

3.1.8. The $^{nat}\text{Dy}(p,xn)^{154m2}\text{Tb}$ reaction

The ^{154}Tb has three long-lived isomeric states. The 22.7 h half-life $^{154m2}\text{Tb}$ isomeric state ($J^\pi = 0^+$), decay-

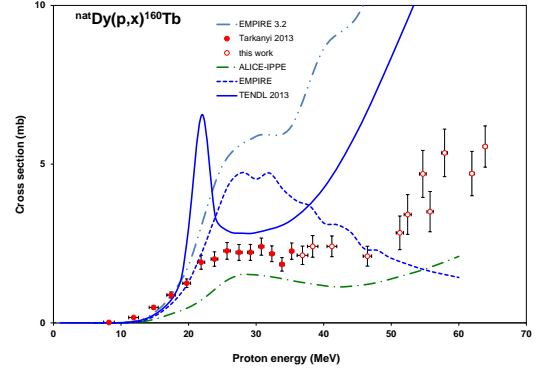


Figure 6: Experimental and theoretical cross sections for the formation of ^{160}Tb by the proton bombardment of dysprosium

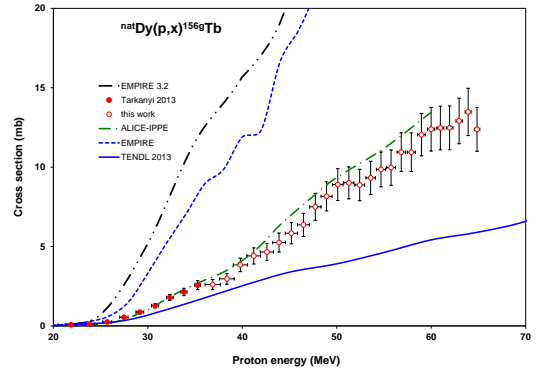


Figure 7: Experimental and theoretical cross sections for the formation of ^{156}Tb by the proton bombardment of dysprosium

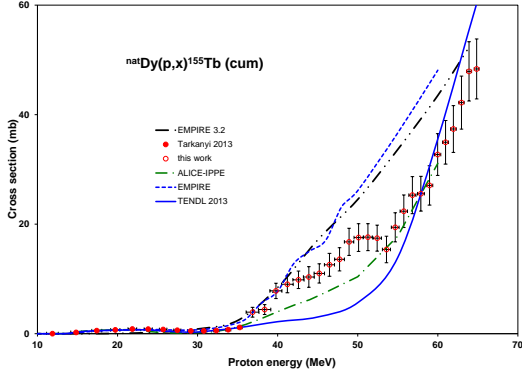


Figure 8: Experimental and theoretical cross sections for the formation of ^{155}Tb by the proton bombardment of dysprosium

ing with 98.2 % $\varepsilon + \beta^+$ to ^{154}Gd , and with 1.8% IT to $^{154m1}\text{Tb}$. The 9.4 h half-life lower lying $^{154m1}\text{Tb}$ isomeric state ($J^\pi = 3^-$) decaying with 78.2 % $\varepsilon + \beta^+$ to ^{154}Gd and with 21.8% IT to ^{154}Gd . The 21.2 h half-life ground state ($J^\pi = 7^-$) decays with 100 % $\varepsilon + \beta^+$ to the stable ^{154}Gd . For production of isomeric states no contribution from the neighboring isobars: ^{154}Dy (alpha emitter) and the ^{154}Gd (stable). Therefore the $^{154m2}\text{Tb}$ isomeric state is produced only directly via (p,2pxn) reactions. The experimental and theoretical cross sections are shown in Fig. 9. The theoretical model codes overestimate the experimental data. In the case of the theoretical calculations of the two isomer states the main problem is connected to the too complex scheme of low-lying levels of ^{154}Tb . There are big gaps at the scheme of gamma-transitions between the lowest levels and it effects directly on the calculated results.

3.1.9. The $^{nat}\text{Dy}(p,xn)^{154m1}\text{Tb}$ reaction

The $^{154m1}\text{Tb}$ ($T_{1/2} = 9.2$ h) is produced directly and via a small branching (1.8 %) from the decay of the $^{154m2}\text{Tb}$ (22.4 h). Taking into account that our spectra were measured after significant cooling time, the effect of the contribution from the isomeric transition can be significant. Therefore the contribution was subtracted. The direct production cross sections are shown in Fig. 10. If we suppose that up to the first spectra around half of the $^{154m2}\text{Tb}$ were decayed, but having only 1.8 %, IT = $0.018 \cdot 0.5$ means only 0.9 % of the $^{154m2}\text{Tb}$. By supposing 9.2 h half-life for this contribution it gives around $3 \cdot 0.9 = 2.7\%$ of the $^{154m2}\text{Tb}$, i.e. 0.03 mb contribution. The theoretical codes underestimate the ex-

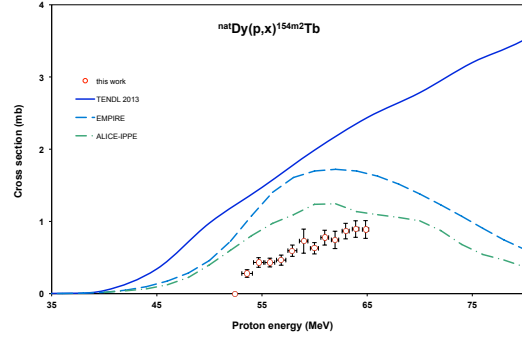


Figure 9: Experimental and theoretical cross sections for the formation of $^{154m2}\text{Tb}$ by the proton bombardment of dysprosium

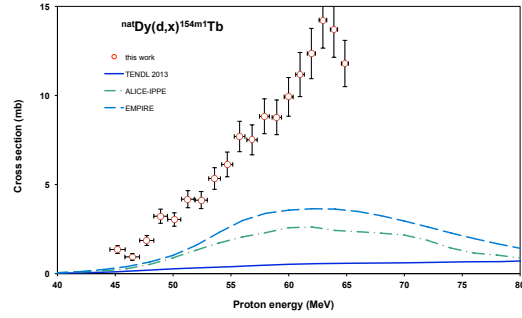


Figure 10: Experimental and theoretical cross sections for the formation of $^{154m1}\text{Tb}$ by the proton bombardment of dysprosium

perimental values and even do not give the same trend. In the cases of ^{154}Tb unfortunately EMPIRE 3.2 does not give isomeric information.

3.1.10. The $^{nat}\text{Dy}(p,xn)^{154g}\text{Tb}$ reaction (cum)

The cross sections were deduced from the first series of spectra measured for around half an hour started in the 22.0-31.6 h after EOB. The results were corrected with the values for $^{154m1}\text{Tb}$, because it was not completely disintegrated into the ground state in the time of the measurements. The experimental results and the nuclear reaction model calculations are given in Fig. 11. The TENDL-2013 approximation gives a bit lower values, all other codes strongly overestimate.

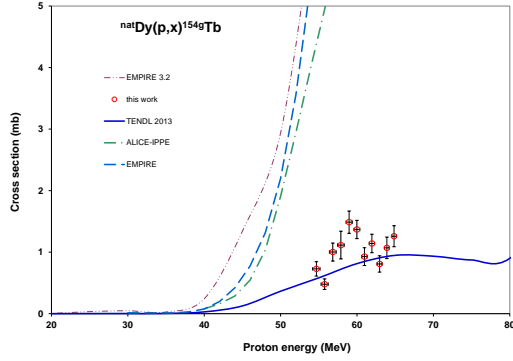


Figure 11: Experimental and theoretical cross sections for the formation of ^{154g}Tb by the proton bombardment of dysprosium

3.1.11. The $^{nat}\text{Dy}(p,xn)^{153}\text{Tb}$ reaction

The cumulative cross sections of the ^{153}Tb ($T_{1/2} = 2.34$ d) were obtained from spectra measured after complete decay of the ^{153}Dy parent ($T_{1/2} = 6.4$ h). The agreement with the TALYS(TENDL-2013) data is acceptable, except the high energy region where the theory underestimates the experiment. (Fig. 12). In this case the EMPIRE 3.2 gives the best and acceptable approximation, while the former EMPIRE version and ALICE-IPPE give overestimating values.

3.1.12. The $^{nat}\text{Dy}(p,xn)^{152}\text{Tb}$ reaction

The measured cross sections of the activation cross section of the ^{152}Tb ($T_{1/2} = 17.5$ h) ground state additional to direct production include the production through the decay of the ^{152m}Tb shorter-lived isomeric state ($T_{1/2} = 4.2$ min, ε : 21.1 %, IT: 78.9 %) and the decay of the parent ^{152}Dy isotope ($T_{1/2} = 2.38$ h, ε : 99.9 %, α : 0.1 %). The agreement with theoretical data in the TENDL library (Fig. 13) is good, up to 60 MeV, from which energy ALICE-IPPE gives better results.

3.1.13. The $^{nat}\text{Dy}(p,xn)^{151}\text{Tb}$ reaction

We obtained only a few cross section data for cumulative cross section of ^{151}Tb ($T_{1/2} = 17.609$ h) near the effective threshold (Fig. 14). The cross sections include the internal decay of the short-lived ^{151m}Tb ($T_{1/2} = 25$ s, IT: 93.4 %, ε : 6.6 %), and of the parent ^{151}Dy ($T_{1/2} = 17.9$ min, α : 5.6 %, ε : 94.4 %). From the theoretical model calculations only the TALYS(TENDL-2013) results show acceptable agreement with the experimental results.

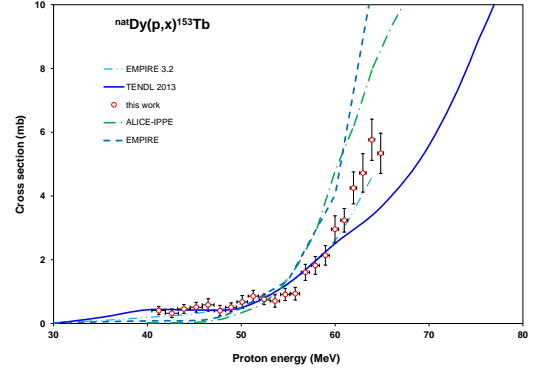


Figure 12: Experimental and theoretical cross sections for the formation of ^{153}Tb by the proton bombardment of dysprosium

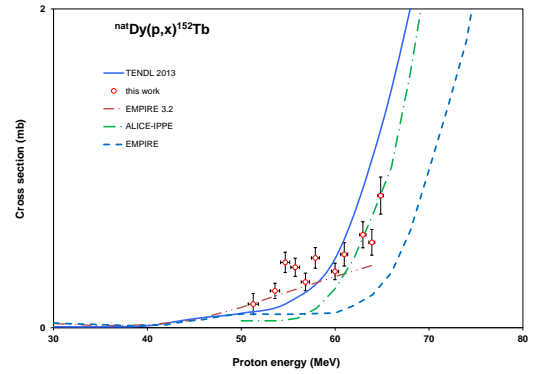


Figure 13: Experimental and theoretical cross sections for the formation of ^{152}Tb by the proton bombardment of dysprosium

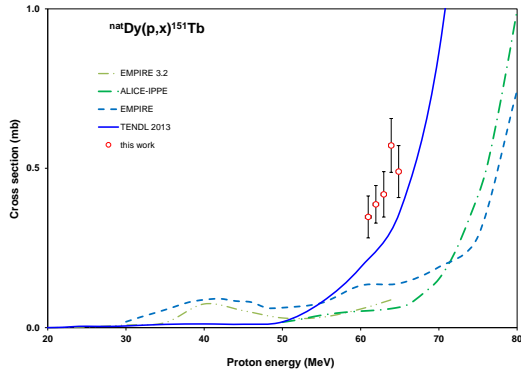


Figure 14: Experimental and theoretical cross sections for the formation of ^{151}Tb by the proton bombardment of dysprosium

3.2. Integral yields

The integral yields calculated from spline fits to our experimental excitation functions are shown in Fig 15 (Dy radioisotopes) and 16. (Tb radioisotopes). The integral yields represent so called physical yields i.e. activity instantaneous production rates (Bonardi, 1987). No experimental thick target yield data were found in the literature for the comparison.

4. Summary and applications

We present new experimental cross sections for the $^{nat}\text{Dy}(p,x)$ ^{159}Dy , ^{157}Dy , ^{155}Dy , ^{161}Tb , ^{160}Tb , ^{156}Tb , ^{155}Tb , $^{154m2}\text{Tb}$, $^{154m1}\text{Tb}$, ^{154g}Tb , ^{153}Tb , ^{152}Tb and ^{151}Tb nuclear reactions in the 36-65 MeV energy range. The experimental data were compared with the results obtained by the TALYS 1.6 code reported in the TENDL-2013 library and with the results of ALICE-IPPE and two versions of the EMPIRE codes. The theoretical description gives only moderate agreements. The comparisons show that the experimental data are very important for testing the predictive power and improving the performances of the model codes, taking into account that no other experimental activation data are available for these reactions. The experimental data are of importance for several practical applications. Among the investigated reaction products we can mention:

- The radionuclide ^{159}Dy ($T_{1/2} = 144$ d, EC =100%) is a pure Auger electron and X-ray emitter and has gained interest in transmission imaging and bone mineral analysis (Nayak and Lahiri, 1999), while

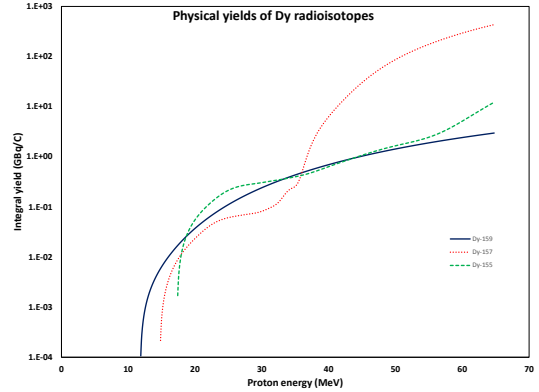


Figure 15: Integral thick target yields for the formation of ^{159}Dy , ^{157}Dy , ^{155}Dy in proton induced nuclear reaction on ^{nat}Dy as a function of the energy

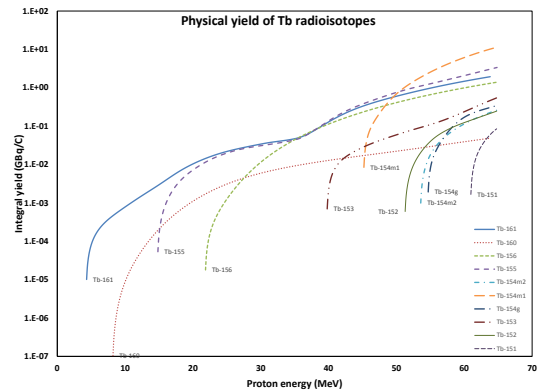


Figure 16: Integral thick target yields for the formation of ^{161}Tb , ^{160}Tb , ^{156}Tb , ^{155}Tb , $^{154m2}\text{Tb}$, $^{154m1}\text{Tb}$, ^{154g}Tb , ^{153}Tb , ^{152}Tb , ^{151}Tb in proton induced nuclear reaction on ^{nat}Dy as a function of the energy

^{157}Dy ($T_{1/2} = 8.14$ h.) (Lebowitz and Greene, 1971), was investigated as a bone seekers in the evaluation of bone lesions (Hubner et al., 1977).

- Terbium offers 4 clinically interesting radioisotopes with complementary physical decay characteristics: ^{149}Tb , ^{152}Tb , ^{155}Tb , and ^{161}Tb . The identical chemical characteristics of these radioisotopes allows the preparation of radiopharmaceuticals with identical pharmaco-kinetics useful for PET (^{152}Tb) or SPECT diagnosis (^{155}Tb) and for α - (^{149}Tb) and β^- -particle (^{161}Tb) therapy (Muller et al., 2012). From Dy targets the ^{152}Tb , ^{155}Tb , and ^{161}Tb can be obtained, but we showed in a recent publication that other production methods are better (Tárkányi et al., 2014a, 2013b).
- Radioisotope Gadolinium (^{153}Gd) is used to manufacture diagnostic sources of photon radiation, in-line sources and calibration phantoms. Because of its magnetic properties, gadolinium is also applied in intravenous radio-contrast agents in magnetic resonance imaging (MRI). There are broad variety of processes to produce the ^{153}Gd with high specific activity. The high radioisotope purity (99.97%) ^{153}Gd can be obtained at high flux reactors via the (n, γ) reaction (Karelin et al., 2000). The charged particle routes include direct and generator methods. The direct route includes proton and deuteron induced reactions on europium (Nichols et al., 1972; Takács et al., 2013) and generator methods via $^{nat}\text{Gd}(p,xn)$ (Vermeulen et al., 2012) $^{nat}\text{Gd}(d,xn)$ (Tárkányi et al., 2014b) and $^{151}\text{Eu}(\alpha,2n)^{153}\text{Tb} \rightarrow ^{153}\text{Gd}$ (Gedeonov et al., 1997) reactions. In principle the presently investigated $^{nat}\text{Dy}(p,x)^{153}\text{Tb} \rightarrow ^{153}\text{Gd}$ also could be taken into account, but the production cross sections by using ^{nat}Dy are very low (see Fig. 13) comparing to other indirect charged particle induced reactions.

5. Acknowledgements

This work was performed in the frame of the HAS-FWO Vlaanderen (Hungary-Belgium) project. The authors acknowledge the support of the research project and of the respective institutions. We thank to Cyclotron Laboratory of the Universit   Catholique in Louvain la Neuve (LLN) providing the beam time and the crew of the LLN Cyclone 90 cyclotron for performing the irradiations. The authors also acknowledge the support from R. Capote (IAEA) in using the newest EMPIRE 3.2 (Malta) version.

References

- Andersen, H. H., Ziegler, J. F., 1977. Hydrogen stopping powers and ranges in all elements. The stopping and ranges of ions in matter, Volume 3. The Stopping and ranges of ions in matter. Pergamon Press, New York.
- Bonardi, M., 1987. The contribution to nuclear data for biomedical radioisotope production from the milan cyclotron facility.
- Canberra, 2000. http://www.canberra.com/products/radiochemistry_lab/genie-2000-software.asp.
- Dityuk, A. I., Konobeyev, A. Y., Lunev, V. P., Shubin, Y. N., 1998. New version of the advanced computer code alice-ippe. Tech. rep., IAEA.
- Gedeonov, A. D., Antropov, A. E., Shkroev, V. Y., 1997. Gd-153 production in the eu-151(alpha,2n)tb-153-gd-153 reaction. Nuclear Instruments & Methods in Physics Research Section A-Accelerators Spectrometers Detectors and Associated Equipment 397 (1), 117–118.
- Herman, M., Capote, R., Carlson, B. V., Oblozinsky, P., Sin, M., Trkov, A., Wienke, H., Zerkin, V., 2007. Empire: Nuclear reaction model code system for data evaluation. Nuclear Data Sheets 108 (12), 2655–2715.
- Herman, M., Capote, R., Sin, M., Trkov, A., Carlson, B., Oblozinsky, P., Mattoon, C., Wienke, H., Hoblit, S., Cho, Y.-S., Plujko, V., Zerkin, V., 2014. Empire-3.2 (malta) <http://www.nndc.bnl.gov/empire>.
- Hermanne, A., Tárkányi, F., Takács, S., 2014. Activation cross sections for production of ^7be by proton and deuteron induced reactions on ^9be : Protons up to 65 mev and deuterons up to 50 mev. Applied Radiation and Isotopes 90 (0), 203–207.
- Hubner, K. F., Andrews, G. A., Hayes, R. L., Poggenburg, J. K., J., Solomon, A., 1977. The use of rare-earth radionuclides and other bone-seekers in the evaluation of bone lesions in patients with multiple myeloma or solitary plasmacytoma. Radiology 125 (1), 171–6.
- International-Bureau-of-Weights-and-Measures, 2000. Guide to the expression of uncertainty in measurement, 1st Edition. International Organization for Standardization, Gen  ve, Switzerland.
- Karelin, Y. A., Efimov, V. N., Filimonov, V. T., Kuznetsov, R. A., Revyakin, Y. L., Andreev, O. I., Zhemkov, I. Y., Bukh, V. G., Lebedev, V. M., Spiridonov, Y. N., 2000. Radionuclide production using a fast flux reactor. Applied Radiation and Isotopes 53 (4-5), 825–827.
- Kinsey, R. R., Dunford, C. L., Tuli, J. K., Burrows, T. W., 1997. in Capture Gamma Ray Spectroscopy and Related Topics, Vol. 2. (NUDAT 2.6 <http://www.nndc.bnl.gov/nudat2/>). Vol. 2. Springer Hungarica Ltd, Budapest.
- Koning, A. J., Rochman, D., 2012. Modern nuclear data evaluation with the talys code system. Nuclear Data Sheets 113, 2841.
- Koning, A. J., Rochman, D., van der Marck, S., Kopecky, J., Sublet, J. C., Pomp, S., Sjostrand, H., Forrest, R., Bauge, E., Henriksson, H., Cabellos, O., Goriely, S., Leppanen, J., Leeb, H., Plompen, A., Mills, R., 2012. Tendl-2013: Talys-based evaluated nuclear data library.
- Lebowitz, E., Greene, M. W., 1971. The production of ^{157}dy for medical use. The International journal of applied radiation and isotopes 22 (12), 789–793.
- May, M., Yaffe, L., 1964. Spallation products produced by bombardment of dysprosium with protons of energies 9-87 mev. Journal of Inorganic and Nuclear Chemistry 26 (4), 479–490.
- Muller, C., Zhernosekov, K., Koster, U., Johnston, K., Dorrer, H., Hohn, A., van der Walt, N. T., Turler, A., Schibli, R., 2012. A unique matched quadruplet of terbium radioisotopes for pet and spect and for alpha- and beta- radionuclide therapy: an in vivo

- proof-of-concept study with a new receptor-targeted folate derivative. *Journal of Nuclear Medicine* 53 (12), 1951–9.
- Nayak, D., Lahiri, S., 1999. Application of radioisotopes in the field of nuclear medicine - i. lanthanide series elements. *Journal of Radioanalytical and Nuclear Chemistry* 242 (2), 423–432.
- Nichols, A. L., Bullock, R. J., Glentworth, P., Large, N. R., 1972. Excitation functions for the formation of various gadolinium and lutetium isotopes by (d,xn) reactions. Tech. rep., Atomic Energy Research Establishment.
- Pritychenko, B., Sonzogni, A., 2003. Q-value calculator.
- Székely, G., 1985. Fgm - a flexible gamma-spectrum analysis program for a small computer. *Computer Physics Communications* 34 (3), 313–324.
- Takács, S., Tárkányi, F., Hermanne, A., Adam-Rebeles, R., Takács, M. P., 2013. Excitation functions for the formation of longer lived isotopes by deuteron irradiation of europium. *Nuclear Instruments & Methods in Physics Research Section B-Beam Interactions with Materials and Atoms* 310, 54–66.
- Tárkányi, F., Ditrói, F., Hermanne, A., Takács, S., Ignatyuk, A. V., 2013a. Investigation of production routes for the ^{161}Ho auger-electron emitting radiolanthanide, a candidate for therapy. *Journal of Radioanalytical and Nuclear Chemistry* 298, 277–286.
- Tárkányi, F., Ditrói, F., Takács, S., Csikai, J., Hermanne, A., Ignatyuk, A. V., 2014a. Activation cross-sections of long lived products of deuteron induced nuclear reactions on dysprosium up to 50 mev. *Applied Radiation and Isotopes* 83, 18–24.
- Tárkányi, F., Ditrói, F., Takács, S., Hermanne, A., Ignatyuk, A. V., 2013b. Activation cross-sections of longer lived products of proton induced nuclear reactions on dysprosium up to 36 mev. *Annals of Nuclear Energy* 62, 375–381.
- Tárkányi, F., Szelecsényi, F., Takács, S., 1991. Determination of effective bombarding energies and fluxes using improved stacked-foil technique. *Acta Radiologica, Supplementum* 376, 72.
- Tárkányi, F., Takács, S., Ditrói, F., Csikai, J., Hermanne, A., Ignatyuk, A. V., 2014b. Activation cross-sections of deuteron induced reactions on gd-nat up to 50 mev. *Applied Radiation and Isotopes* 83, 25–35.
- Tárkányi, F., Takács, S., Gul, K., Hermanne, A., Mustafa, M. G., Nortier, M., Oblozinsky, P., Qaim, S. M., Scholten, B., Shubin, Y. N., Youxiang, Z., 2001. Beam monitor reactions (chapter 4). charged particle cross-section database for medical radioisotope production: diagnostic radioisotopes and monitor reactions. Tech. rep., IAEA.
- Vermeulen, C., Steyn, G. F., Szelecsényi, F., Kovács, Z., Suzuki, K., Nagatsu, K., Fukumura, T., Hohn, A., van der Walt, T. N., 2012. Cross sections of proton-induced reactions on gd-nat with special emphasis on the production possibilities of ^{152}Tb and ^{155}Tb . *Nuclear Instruments & Methods in Physics Research Section B-Beam Interactions with Materials and Atoms* 275, 24–32.

Table 2: Decay characteristics of the investigated reaction products and Q-values of reactions for their productions

Nuclide	Half-life	E_{γ} (keV)	I_{γ} (%)	Contributing reaction	Q-value(keV)
¹⁵⁹ Dy EC: 100 %	144.4 d	58.0	2.27	¹⁶⁰ Dy(p,pn) ¹⁶¹ Dy(p,p2n) ¹⁶² Dy(p,p3n) ¹⁶³ Dy(p,p4n) ¹⁶⁴ Dy(p,p5n) ¹⁵⁹ Ho decay	-8575.9 -15030.29 -23227.29 -29498.3 -37156.42 -11195.85
¹⁵⁷ Dy EC: 100 %	8.14 h	182.424 326.336	1.3393	¹⁵⁸ Dy(p,pn) ¹⁶⁰ Dy(p,p3n) ¹⁶¹ Dy(p,p4n) ¹⁶² Dy(p,p5n) ¹⁶³ Dy(p,p6n) ¹⁶⁴ Dy(p,p7n) ¹⁵⁷ Ho decay	-9055.54 -24464.14 -30918.53 -39115.52 -45386.54 -53044.66 -12429.3
¹⁵⁵ Dy EC: 98.62 % β^+ : 1.38 %	9.9 h	184.564 226.918	3.37 68.4	¹⁵⁸ Dy(p,p3n) ¹⁶⁰ Dy(p,p5n) ¹⁶¹ Dy(p,p6n) ¹⁶² Dy(p,p7n) ¹⁶³ Dy(p,p8n) ¹⁶⁴ Dy(p,p9n) ¹⁵⁵ Ho decay	-25466.2 -40874.7 -47329.1 -55526.1 -61797.1 -69455.3 -13342.8
¹⁶¹ Tb β^- : 100 %	6.89 d	74.56669 87.941 103.065 106.113 292.401	10.2 0.183 0.101 0.078 0.058	¹⁶² Dy(p,2p) ¹⁶³ Dy(p,2pn) ¹⁶⁴ Dy(p,2p2n)	-8007.59 -14278.6 -21936.72
¹⁶⁰ Tb β^- : 100 %	72.3 d	86.7877 298.5783 879.378 966.166 1177.954	13.2 26.1 30.1 25.1 14.9	¹⁶¹ Dy(p,2p) ¹⁶² Dy(p,2pn) ¹⁶³ Dy(p,2p2n) ¹⁶⁴ Dy(p,2p3n)	-7507.17 -15704.16 -21975.17 -29633.29
¹⁵⁶ Tb ϵ : 100 %	5.35 d	88.97 199.19 262.54 296.49 356.38 422.34 534.29 1065.11 1154.07 1222.44	18 41 5.8 4.5 13.6 8.0 67 10.8 10.431	¹⁵⁸ Dy(p,2pn) ¹⁶⁰ Dy(p,2p3n) ¹⁶¹ Dy(p,2p4n) ¹⁶² Dy(p,2p5n) ¹⁶³ Dy(p,2p6n) ¹⁶⁴ Dy(p,2p7n)	-15674.87 -31083.47 -37537.86 -45734.85 -52005.87 -59663.98
¹⁵⁵ Tb EC: 100 %	5.32 d	86.55 105.318 148.64 161.29 163.28 180.08 262.27	32.0 25.1 2.65 2.76 4.44 7.5 5.3	¹⁵⁶ Dy(p,2p) ¹⁵⁸ Dy(p,2p2n) ¹⁶⁰ Dy(p,2p4n) ¹⁶¹ Dy(p,2p5n) ¹⁶² Dy(p,2p6n) ¹⁶³ Dy(p,2p7n) ¹⁶⁴ Dy(p,2p8n) ¹⁵⁵ Dy decay	-6567.84 -22589.3 -37997.9 -44452.3 -52649.3 -58920.3 -66578.4 -13342.8
^{154m2} Tb $\epsilon + \beta^+$: 98.2 % IT: 1.8 %	22.7 h	123.071 247.925 346.643 992.92 1419.81	43 79 69 16.2 46	¹⁵⁶ Dy(p,2pn) ¹⁵⁸ Dy(p,2p3n) ¹⁶⁰ Dy(p,2p5n) ¹⁶¹ Dy(p,2p6n) ¹⁶² Dy(p,2p7n) ¹⁶³ Dy(p,2p8n)	-15732.9 -31753.4 -47161.3 -53615.7 -61812.7 -68083.7
^{154m1} Tb $\epsilon + \beta^+$: 78.2 % IT: 21.8 %	9.4 h	247.925 540.18 649.564 873.190 996.262	22.1 20 10.9 9.2 8.6	¹⁵⁶ Dy(p,2pn) ¹⁵⁸ Dy(p,2p3n) ¹⁶⁰ Dy(p,2p5n) ¹⁶¹ Dy(p,2p6n) ¹⁶² Dy(p,2p7n) ¹⁶³ Dy(p,2p8n)	-15732.9 -31753.4 -47161.3 -53615.7 -61812.7 -68083.7
^{154g} Tb EC: 97.6 % β^+ : 2.4 %	21.5 h	123.07 557.60 722.12 1123.09 1274.436 1291.31	26.54 7.7 5.7 10.5 6.9	¹⁵⁶ Dy(p,2pn) ¹⁵⁸ Dy(p,2p3n) ¹⁶⁰ Dy(p,2p5n) ¹⁶¹ Dy(p,2p6n) ¹⁶² Dy(p,2p7n) ¹⁶³ Dy(p,2p8n)	-15732.9 -31753.4 -47161.3 -53615.7 -61812.7 -68083.7
¹⁵³ Tb EC: 9.906 % β^+ : 0.094 %	2.34 d	102.255 109.75 170.42 212.00	6.4 6.8 6.3 31.0	¹⁵⁶ Dy(p,2p2n) ¹⁵⁸ Dy(p,2p4n) ¹⁶⁰ Dy(p,2p6n) ¹⁶¹ Dy(p,2p7n) ¹⁶² Dy(p,2p8n) ¹⁶³ Dy(p,2p9n) ¹⁵³ Dy decay	-22647.0 -38667.46 -54075.37 -60529.76 -68726.74 -74997.76 -25599.71
¹⁵² Tb ϵ : 79.7 % β^+ : 20.3 %	17.5 h	271.09 344.2785 778.9045	9.53 63.5 5.54	¹⁵⁶ Dy(p,2p3n) ¹⁵⁸ Dy(p,2p5n) ¹⁶⁰ Dy(p,2p7n) ¹⁶¹ Dy(p,2p8n) ¹⁶² Dy(p,2p9n) ¹⁵² Dy decay	-31315.0 -47335.4 -62743.3 -69197.7 -77394.7 -32695.67
¹⁵¹ Tb EC: 99.91 % β^+ : 0.99 % α : 0.0095 %	17.609 h	108.088 180.186 251.863 287.357 395.444 443.879 479.357 587.46 616.561	24.3 11.5 26.3 28.3 10.8 10.8 15.4 15.6 10.4	¹⁵⁶ Dy(p,2p4n) ¹⁵⁸ Dy(p,2p6n) ¹⁶⁰ Dy(p,2p8n) ¹⁶¹ Dy(p,2p9n) ¹⁵¹ Dy decay	-38479.64 -54500.1 -69907.99 -76362.38 -42132.82

Naturally occurring dysprosium is composed of 7 isotopes (¹⁵⁶Dy-0.06 %, ¹⁵⁸Dy-0.10 %, ¹⁶⁰Dy-2.34 %, ¹⁶¹Dy-18.9 %, ¹⁶²Dy-25.5 %, ¹⁶³Dy-24.9 % and ¹⁶⁴Dy-28.2 %).

When complex particles are emitted instead of individual protons and neutrons the Q-values have to be decreased by the respective binding energies of the compound particles: np-d, +2.2 MeV; 2np-t, +8.48 MeV; n2p-³He, +7.72 MeV; 2n2p- α , +28.30 MeV

Table 3: Experimental cross sections of $^{nat}\text{Dy}(p,xn)^{159}\text{Dy}$, ^{157}Dy , ^{155}Dy , ^{161}Tb , ^{160}Tb , ^{156}Tb , and ^{155}Tb reactions

$E \pm \delta E$ (MeV)	^{159}Dy		^{157}Dy		^{155}Dy		^{161}Tb		^{160}Tb		^{156}Tb		^{155}Tb		
	$\sigma \pm \delta\sigma(\text{mb})$														
36.9	0.8	323.9	41.0	16.3	1.8	0.6	0.1	12.6	1.4	2.1	0.3	2.6	0.3	3.9	0.9
38.4	0.8	363.5	43.1	21.4	2.3	0.8	0.1	10.7	1.2	2.4	0.3	3.0	0.3	4.4	0.9
39.8	0.8	371.7	46.9	29.4	3.2	0.9	0.1					3.8	0.4	7.8	1.4
41.2	0.7	351.1	44.3	41.7	4.5	1.0	0.1	12.0	1.3	2.4	0.3	4.4	0.5	9.0	1.6
42.6	0.7	352.7	43.3	58.9	6.4	1.0	0.1	14.1	1.6			4.7	0.5	9.8	1.6
43.9	0.7	409.7	51.4	80.4	8.7	1.3	0.2					5.2	0.6	10.4	1.9
45.2	0.7	429.3	52.5	100.7	10.9	1.3	0.2	4.9	0.6			5.8	0.7	11.0	1.8
46.5	0.6	457.3	56.4	121.1	13.1	1.4	0.2	9.8	1.1	2.1	0.3	6.4	0.7	12.6	2.1
47.7	0.6	425.2	52.4	137.3	14.9	1.4	0.2	12.2	1.4			7.5	0.9	13.6	2.1
48.9	0.6	404.8	50.0	155.6	16.8	1.4	0.2	14.4	1.6			8.2	0.9	16.8	2.5
50.1	0.6	543.3	64.9	170.1	18.4	1.4	0.2					8.9	1.0	17.6	2.5
51.3	0.5	432.0	52.7	183.9	19.9	1.4	0.2	14.6	1.6	2.8	0.5	9.0	1.0	17.6	2.5
52.4	0.5	475.7	57.6	188.5	20.4	1.5	0.2	18.9	2.1	3.4	0.6	8.9	1.0	17.4	2.4
53.6	0.5	389.5	50.4	199.5	21.6	2.0	0.2					9.3	1.0	15.4	2.4
54.7	0.5	423.9	53.2	208.5	22.6	2.4	0.3	20.7	2.3	4.7	0.7	9.9	1.1	19.4	2.7
55.8	0.5	522.0	64.3	221.9	24.0	3.1	0.3	19.7	2.2	3.5	0.6	10.0	1.1	22.4	3.0
56.8	0.4	405.2	52.8	231.4	25.0	4.3	0.5					10.9	1.2	25.3	3.4
57.9	0.4	526.4	63.3	244.2	26.4	5.6	0.6	19.6	2.2	5.4	0.7	10.9	1.2	25.6	3.2
59.0	0.4	463.7	58.4	257.0	27.8	7.1	0.8					12.0	1.3	27.1	3.6
60.0	0.4	411.6	52.1	263.6	28.5	8.8	1.0					12.4	1.4	32.7	3.8
61.0	0.4	468.8	58.0	273.6	29.6	10.8	1.2					12.5	1.4	35.0	4.0
61.9	0.4	404.2	52.3	280.7	30.4	13.0	1.4	23.9	2.6	4.7	0.7	12.5	1.4	37.4	4.3
63.0	0.3	463.6	59.0	287.9	31.1	15.9	1.7					12.9	1.4	42.2	4.8
63.9	0.3	458.8	60.1	299.3	32.4	19.9	2.2	24.9	2.7	5.6	0.7	13.5	1.5	47.9	5.4
64.9	0.3	569.7	70.8	271.4	29.4	20.7	2.3	5.4	0.7			12.4	1.4	48.3	5.5

Table 4: Experimental cross sections $^{154m2}\text{Tb}$, $^{154m1}\text{Tb}$, ^{154g}Tb , ^{153}Tb , ^{152}Tb and ^{151}Tb reactions

$E \pm \delta E$ (MeV)	$^{154m2}\text{Tb}$		$^{154m1}\text{Tb}$		^{154g}Tb		^{153}Tb		^{152}Tb		^{151}Tb		
	$\sigma \pm \delta\sigma(\text{mb})$												
36.9	0.8												
38.4	0.8												
39.8	0.8						1.07	0.28					
41.2	0.7						0.41	0.13					
42.6	0.7						0.32	0.14					
43.9	0.7						0.46	0.14					
45.2	0.7			1.35	0.22		0.51	0.15					
46.5	0.6			0.94	0.19		0.58	0.19					
47.7	0.6			1.86	0.27		0.40	0.17					
48.9	0.6			3.22	0.40		0.51	0.14					
50.1	0.6			3.04	0.38		0.68	0.20					
51.3	0.5			4.18	0.48		0.86	0.18	0.15	0.07			
52.4	0.5			4.13	0.48		0.76	0.17					
53.6	0.5	0.28	0.05	5.34	0.61		0.71	0.20	0.23	0.05			
54.7	0.5	0.43	0.07	6.13	0.70	0.73	0.14	0.91	0.19	0.41	0.06		
55.8	0.5	0.43	0.06	7.70	0.86	0.48	0.10	0.94	0.20	0.38	0.06		
56.8	0.4	0.46	0.07	7.51	0.84	1.00	0.18	1.60	0.25	0.29	0.06		
57.9	0.4	0.59	0.08	8.83	0.98	1.12	0.27	1.82	0.28	0.44	0.06		
59.0	0.4	0.73	0.17	8.77	0.98	1.49	0.22	2.14	0.31				
60.0	0.4	0.63	0.08	9.92	1.08	1.37	0.18	2.96	0.42	0.35	0.05		
61.0	0.4	0.78	0.10	11.2	1.2	0.93	0.17	3.24	0.37	0.46	0.07	0.35	0.07
61.9	0.4	0.74	0.12	12.4	1.4	1.14	0.18	4.25	0.50			0.39	0.06
63.0	0.3	0.87	0.11	14.2	1.6	0.81	0.16	4.72	0.60	0.58	0.08	0.42	0.07
63.9	0.3	0.89	0.11	13.7	1.6	1.07	0.21	5.76	0.65	0.54	0.08	0.57	0.08
64.9	0.3	0.89	0.12	11.8	1.3	1.26	0.21	5.34	0.63	0.83	0.12	0.49	0.08